Available online at www.sciencedirect.com
ScienceDirect
Journal of Sound and Vibration 310 (2008) 58–76
JOURNAL OF SOUND AND VIBRATION
www.elsevier.com/locate/jsvi

Waves in thin-walled fluid-filled ducts with arbitrary cross-sections

C.-M. Nilsson*, S. Finnveden

MWL, Aeronautical and Vehicle Engineering, KTH, SE-100 44 Stockholm, Sweden

Received 31 August 2004; received in revised form 16 May 2007; accepted 18 July 2007
Available online 31 October 2007

Abstract

First, a variational formulation for fluid–shell coupling is presented. Subsequently new waveguide finite elements for fluid and fluid–shell coupling are derived from this formulation. Together with previously derived elements, modelling thin-walled shells, equations for pipes and ducts with arbitrary cross-sections may be formulated. Two examples, one pipe and one duct, are presented together with dispersion curves for the respective case.

1. Introduction

Analyses of the wave motion in fluid-filled ducts and pipes is important both for studying acoustic energy propagation and radiation. Generally a wave is propagating both in the fluid and in the structure. The coupling between the fluid and the shell is thus of great importance. For lightly coupled systems fluid–structure coupling may be simplified, but often fully coupled systems must be considered.

For pipes, 'circular ducts', the circular symmetry may be utilized by using a trigonometric dependence with respect to the circumferential coordinate. Then, for fluid-filled pipes, results may be obtained as presented by, e.g., Fuller and Fahy [1] or Finnveden [2] and in simplified form by Pavić [3].

For arbitrary cross-sections more general methods are required. One method, based on slices of ordinary finite elements has been used by Maess et al. [4] for deriving dispersion relations for fluid-filled pipes. With this method, discrete equations are devised by conventional finite element models which subsequently are post-processed.

In this paper another generic method for obtaining equations describing waves for fully coupled pipes and ducts with arbitrary cross-sections is presented. This method is here referred to as the waveguide finite element (WFE) method. The resulting equations may be used to give dispersion relations as shown in this paper. But also calculations of group velocities [5], response of infinite pipes or ducts [6] and coupling to ordinary finite elements [7] are within the scope of the method.

The WFE technique has previously been used to obtain system equations for several different cases, including orthotropic solids [8], fully anisotropic solids, [9], fluid–shell systems [10,11], fluids with stationary

*Corresponding author. Current address: GRUNDFOS Management A/S, Poul Due Jensens Vej 7, DK 8850, Denmark.
E-mail addresses: cnilsson@grundfos.com (C.-M. Nilsson), svantef@kth.se (S. Finnveden).

0022-460X/$ - see front matter
doi:10.1016/j.jsv.2007.07.081

flow, [12], thin-walled-shells [13] and prestressed anisotropic shells [14]. The prerequisites of the WFE-method is to assume constant properties along one direction. The properties with respect to the cross-section geometry is then modelled with finite elements. Upon this basis follows a system of coupled equations for propagation along the waveguide. Wave-solutions with respect to the direction of propagation, for arbitrary cross-sectional geometry are consequently found from a polynomial eigenproblem, as discussed in Section 6 of this paper.

Here it should be recognized that elements derived by Astley et al. [10,11], also describe waves in fluid–shell coupled systems, and thus are quite similar to those presented here. However, the current method differs in some respects. The most important of these is that the shell (or more precisely plate–strip) elements used here include in-plane motion. Such in-plane motion is necessary to describe low order bending waves of the entire structure. In-plane motion of the shell is also needed for the 'breathing' motion in pipes, see e.g. Ref. [1], and similarly in-plane motion in flat–oval ducts, as discussed by Cummings [15].

Shell elements similar to those used here were first introduced by Gavric [13]. To better capture the coupling between in-plane and out-of-plane motion, quadratic interpolation of the in-plane motion is used instead of linear interpolation. Also a 'trick' employed in Ref. [13] to make the resulting, undamped, eigenproblem real valued is not considered here. Instead the presented formulation gives complex Hermitian eigenproblems for undamped shells.

The fluid motion is here treated in terms of the fluid's velocity potential rather than the pressure. This yields a 'gyroscopic' coupled system which enables an orthogonal basis of eigenvectors for the expanded system to be found as discussed in Ref. [14, Chapter 1]. For simplicity, the fluid elements presented here are linear triangular since these elements are more flexible in meshing surfaces with complex geometry and tools for automatic meshing of arbitrary areas are readily available. The main drawback of this choice is a slower rate of convergence. Finally, the elements presented here are given both in a 'weak form' and a 'strong form', which should enable future implementation of 'Super Spectral Elements' derived from the models presented here, see Ref. [7].

The 'finite slice' method, or discrete waveguide FE method, used by Maess et al. [4] has attracted some attention recently, e.g. Refs. [16,17]. An advantage with this method is that existing conventional FE programs can be used and there is no need for new element formulations. A disadvantage is that the method is affected by numerical problems such as ill-conditioning and round-of errors [18]. Some of these numerical problems are avoided with the waveguide FEM advocated in this article, as it provides continuous equations in the direction along the waveguide. The method, however, requires new finite elements and the major contribution of the present article is two new elements that greatly increases the class of structures for which the method can be used.

The presented work is subdivided as follows. A variational formulation for fluid–shell coupling is derived. Subsequently, waveguide finite elements for plate-strips, fluids and fluid–shell coupling are presented. Then dispersion curves for two examples are given. First, a water-filled steel pipe is considered. For this pipe a validation with a method presented in Ref. [2] is made. Second, dispersion curves for a water-filled steel duct with dimensions according to the EN 10219 standard for hollow steel profiles, see e.g. Ref. [19], are presented and discussed.

2. Variational description of fluid–shell coupling

Formulations describing a structures coupling to a fluid which is described with a fluid potential is presented in e.g. Refs. [20,21]. The method presented here has been used in Ref. [2] and has the advantages of describing the undamped coupled system with Hermitian matrices and also making the matrix proportional to the squared frequency positive definite. The following short derivation of this coupling is more straightforward than that in Ref. [2].

Consider harmonic motion of the form, $e^{i\omega t}$, where ω is the angular frequency and t is the time. For a fluid surrounded by a shell, a modified version of Hamilton's principle, [22, Chapter 1], may then be written as

$$\delta(U_f - T_f) - \delta W_f = 0, \tag{1}$$

where δ symbolizes first variation. U_f is the potential and T_f is the kinetic energy in the fluid. δW_f symbolizes the virtual work on the fluid. The corresponding equation for the shell is equivalent to Eq. (1) except for a

change of indices 's', referring to the shell instead of 'f', referring to the fluid. Thus,

$$\delta(U_s - T_s) - \delta W_s = 0, \tag{2}$$

where U_s is the potential and T_s is the kinetic energy in the shell and δW_s symbolizes the virtual work on the shell. For the purpose of this paper the virtual work in each case is solely due to the coupling between the fluid and the shell. Now, any functional defined by a linear combination of Eqs. (1) and (2) defines a functional for the combined system. Here, Eq. (2) is subtracted from Eq. (1). This choice has some useful properties elaborated in Section 6. The result may be written as

$$\delta L_s + \delta L_f + \delta B_c = 0, \tag{3}$$

where

$$\delta L_s = \delta(U_s - T_s) \tag{4}$$

is a bilinear functional for the shell

$$\delta L_f = -\delta(U_f - T_f) \tag{5}$$

is a bilinear functional for the fluid and

$$\delta B_c = \delta W_f - \delta W_s \tag{6}$$

is a functional representing the boundary coupling. δL_s is used in the derivation of the shell elements. δL_f is used in the derivation of the fluid elements and δB_c is used for deriving the fluid–shell coupling elements.

Details of the boundary coupling term, δB_c, are explored in the following. To begin, the virtual work on the shell from the fluid is given by

$$\delta W_s = \int_S \delta w^* p \, \mathrm{d}S, \tag{7}$$

where δw, is the virtual displacement of the shell out of the fluid, $*$ denotes complex conjugate, S is the wetted surface of the fluid shell boundary and p is the fluid pressure. Correspondingly, the virtual work on the fluid from the shell is given by

$$\delta W_f = -\int_S \delta p^* w \, \mathrm{d}S. \tag{8}$$

Energy flow into the shell is defined to be positive by Eq. (7). The energy flow into the fluid is opposite to that into the shell, which explains the minus sign in Eq. (8). For the acoustic wave equation the fluid velocity is written in terms of a velocity potential, ψ, see Ref. [23]. Consequently,

$$\mathrm{i}\omega \mathbf{u}_f = -\nabla\psi, \tag{9}$$

where $\mathbf{u}_f$ is the fluid particle displacement. In terms of this velocity potential, the pressure is given by

$$p = \mathrm{i}\omega\rho_f\psi, \tag{10}$$

where ρ_f is the fluid density at equilibrium. Hence, the coupling term, δB_c is written as

$$\delta B_c = \mathrm{i}\omega \int_S \rho_f(\delta\psi^* w - \delta w^* \psi) \, \mathrm{d}S. \tag{11}$$

Eq. (11) is used in Section 5 for deriving fluid–shell coupling waveguide finite elements.

3. Plate-strip elements

Plate-strip elements can be used to build up complex shaped shell structures. The derivation of the plate-strip elements used here is shortly treated in the following. More thorough analysis may be found in Refs. [5,14]. Similar elements have been reported in Refs. [13,24,7].

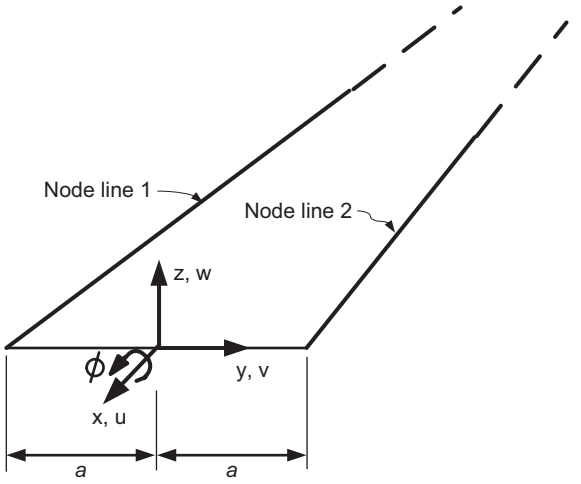

Fig. 1. Plate-strip element.

Consider a plate strip with displacements u, v and w and a rotation ϕ as shown in Fig. 1. Such plate strips may be used to build up shell structures with arbitrary cross-sectional geometry. Hence, they may alternatively be referred to as shell elements.

3.1. First variation of potential energy

For a thin isotropic plate, the first variation of the potential energy in the frequency domain may be written as

$$\delta U = \int_S [\delta\boldsymbol{\varepsilon}^H \quad \delta\kappa^H][\mathbf{D}]\begin{bmatrix}\boldsymbol{\varepsilon}\\ \boldsymbol{\varkappa}\end{bmatrix} \mathrm{d}S, \tag{12}$$

where H denotes complex conjugate transpose and

$$[\mathbf{D}] = \frac{h}{1-v^2}\begin{bmatrix}\mathbf{D}_1 & \\ & \frac{h^2}{12}\mathbf{D}_1\end{bmatrix}, \tag{13}$$

$$[\mathbf{D}_1] = \begin{bmatrix}E & vE & 0\\ vE & E & 0\\ 0 & 0 & (1-v^2)G\end{bmatrix}. \tag{14}$$

E denotes Young's modulus, v denotes Poisson's ratio, $G = E/2(1+v)$ is the shear modulus and h is the thickness of the plate.

$\boldsymbol{\varepsilon}$ is the in-plane strain at the neutral layer of the plate strips and $\boldsymbol{\varkappa}$ is the curvature of the plate strip relative to its undeformed state. These strains and curvatures are related to the displacements through,

$$\boldsymbol{\varepsilon} = \begin{bmatrix}\frac{\partial u}{\partial x}\\ \frac{\partial v}{\partial y}\\ \frac{\partial u}{\partial y}+\frac{\partial v}{\partial x}\end{bmatrix} \quad \text{and} \quad \boldsymbol{\varkappa} = \begin{bmatrix}-\frac{\partial^2 w}{\partial x^2}\\ -\frac{\partial^2 w}{\partial y^2}\\ -2\frac{\partial^2 w}{\partial x \partial y}\end{bmatrix}. \tag{15}$$

3.2. First variation of kinetic energy

The first variation of the kinetic energy in the frequency domain is written as

$$\delta T_s = \omega^2 \int_S [\delta u^* \;\; \delta v^* \;\; \delta w^*][\mathbf{M}_s] \begin{bmatrix} u \\ v \\ w \end{bmatrix} \mathrm{d}S, \tag{16}$$

where

$$[\mathbf{M}_s] = \begin{bmatrix} m'' & & \\ & m'' & \\ & & m'' \end{bmatrix} \tag{17}$$

and m'' is the mass per unit area of the shell.

3.3. Shape function approximations

The elements used here approximate the out-of-plane motion with third degree polynomial shape-functions whereas second degree polynomials are used for the in-plane motion. Thus the displacements are approximated as

$$u = \mathbf{N}_p^{\mathrm{T}}(\vartheta)\hat{\mathbf{u}}(x), \quad \delta u^* = \delta\hat{\mathbf{u}}(x)^H \mathbf{N}_p(\vartheta), \tag{18}$$

$$v = \mathbf{N}_p^{\mathrm{T}}(\vartheta)\hat{\mathbf{v}}(x), \quad \delta v^* = \delta\hat{\mathbf{v}}(x)^H \mathbf{N}_p(\vartheta), \tag{19}$$

$$w = \mathbf{N}_b^{\mathrm{T}}(\vartheta)\hat{\mathbf{w}}(x), \quad \delta w^* = \delta\hat{\mathbf{w}}(x)^H \mathbf{N}_b(\vartheta), \tag{20}$$

where

$$\hat{\mathbf{u}} = [\hat{u}_1 \;\; \hat{u}_2 \;\; \hat{u}_3]^{\mathrm{T}}, \quad \hat{\mathbf{v}} = [\hat{v}_1 \;\; \hat{v}_2 \;\; \hat{v}_3]^{\mathrm{T}}, \quad \hat{\mathbf{w}} = [\hat{w}_1 \;\; \hat{\phi}_1 \;\; \hat{w}_2 \;\; \hat{\phi}_2]^{\mathrm{T}}, \tag{21}$$

$$\delta\hat{\mathbf{u}} = [\delta\hat{u}_1 \;\; \delta\hat{u}_2 \;\; \delta\hat{u}_3]^{\mathrm{T}}, \quad \delta\hat{\mathbf{v}} = [\delta\hat{v}_1 \;\; \delta\hat{v}_2 \;\; \delta\hat{v}_3]^{\mathrm{T}}, \quad \delta\hat{\mathbf{w}} = [\delta\hat{w}_1 \;\; \delta\hat{\phi}_1 \;\; \delta\hat{w}_2 \;\; \delta\hat{\phi}_2]^{\mathrm{T}}. \tag{22}$$

The sub-indices, 1 and 2 indicate the values of the displacements, u, v, w, or rotations ϕ along the respective node-line as shown in Fig. 1. The sub-index 3 refers to an internal 'bubble' degree of freedom associated with a quadratic shape-function, similar to that described by Cook [25, p. 178]. The shape-functions are given by

$$\mathbf{N}_p(\vartheta) = \begin{bmatrix} \frac{1}{2}(1-\vartheta) \\ \frac{1}{2}(1+\vartheta) \\ (1-\vartheta^2) \end{bmatrix} \quad \text{and} \quad \mathbf{N}_b(\vartheta) = \begin{bmatrix} \frac{1}{4}(2-3\vartheta+\vartheta^3) \\ \frac{a}{4}(1-\vartheta-\vartheta^2+\vartheta^3) \\ \frac{1}{4}(2+3\vartheta-\vartheta^3) \\ \frac{a}{4}(-1-\vartheta+\vartheta^2+\vartheta^3) \end{bmatrix}, \tag{23}$$

where $\vartheta = y/a$ in the local coordinate system shown in Fig. 1. The above displacement assumptions are inserted into Eqs. (12) and (16) after which the integration over the width of the shell is calculated. The resulting approximation of δL_s for the element is written as

$$\delta L_s \approx \int \sum_{k=0}^{2} \sum_{l=0}^{2} \frac{\partial^k \delta\hat{\mathbf{W}}^H}{\partial^k} \mathbf{a}_{kl} \frac{\partial^l \hat{\mathbf{W}}}{\partial x^l} - \omega^2 \delta\hat{\mathbf{W}}^H \mathbf{m}_2 \hat{\mathbf{W}} \, \mathrm{d}x, \tag{24}$$

where

$$\hat{\mathbf{W}} = [\hat{\mathbf{u}}^{\mathrm{T}} \;\; \hat{\mathbf{v}}^{\mathrm{T}} \;\; \hat{\mathbf{w}}^{\mathrm{T}}]^{\mathrm{T}} \tag{25}$$

and

$$\delta\hat{\mathbf{W}} = [\delta\hat{\mathbf{u}}^{\mathrm{T}} \;\; \delta\hat{\mathbf{v}}^{\mathrm{T}} \;\; \delta\hat{\mathbf{w}}^{\mathrm{T}}]^{\mathrm{T}}. \tag{26}$$

4. Fluid elements

Taking the first variation of expressions for U_f and T_f in the frequency domain gives a bilinear functional for the fluid. For the acoustic wave equation these expressions may by found in e.g. Ref. [23]. The result is

$$\delta L_f = \int \rho_f \nabla\delta\psi^H \nabla\psi - \omega^2 \frac{\rho_f}{c_f^2} \delta\psi^* \psi \, \mathrm{d}V, \tag{27}$$

where H denotes complex conjugate transpose and c_f is the fluid sound speed for plane waves. In the following, the coefficients ρ_f and c_f are considered to be constant within each waveguide finite element.

The cross-sections of the fluid elements are chosen to be triangular and the velocity potential approximation over an element's cross-section is linear. Finite elements with these properties are common, see for instance Ref. [25, Chapter 5]. The advantage with this type of triangular element is that meshing software, such as the MATLAB pde-toolbox, utilized here, is readily available and easily meshes arbitrary cross-sectional shapes. Furthermore, the element type is simple and well proven. The main drawback of the elements is their slow convergence to exact solutions due to a coarse approximation by the linear shape approximation space.

4.1. Triangular coordinates and shape-functions

The cross-section of a single element is seen in Fig. 2. Triangular coordinates, ξ_i for $i = 1, 2, 3$, are defined as the ratios between the triangle sub-areas, A_1, A_2, A_3 and the total area, A, see also Ref. [25]. Thus,

$$\xi_i = \frac{A_i}{A}, \tag{28}$$

where

$$A = A_1 + A_2 + A_3. \tag{29}$$

The triangular elements relation to the global coordinate system is seen in Fig. 3.

The values of ψ at the node-lines 1, 2 and 3 in Fig. 2 are denoted by $\hat{\psi}_i$, $i = 1, 2, 3$. With linear interpolation, the value of ψ at any point within the element is given by

$$\psi = \mathbf{N}_f^{\mathrm{T}} \hat{\boldsymbol{\psi}}(x), \tag{30}$$

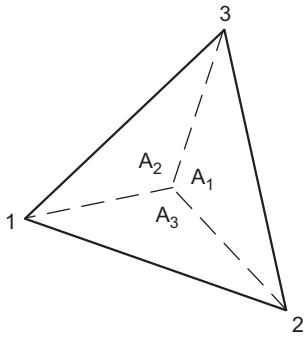

Fig. 2. Triangle coordinates.

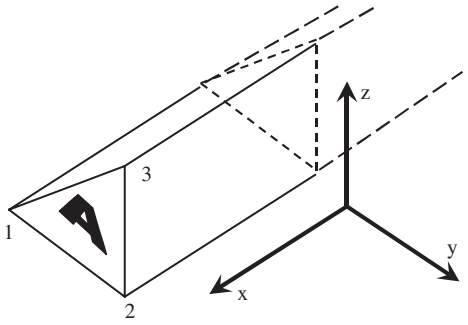

Fig. 3. Fluid waveguide element within global coordinates. A is the (total) cross-section area.

where

$$\mathbf{N}_f = \begin{bmatrix} \xi_1 \\ \xi_2 \\ \xi_3 \end{bmatrix} \quad \text{and} \quad \hat{\boldsymbol{\psi}}(x) = \begin{bmatrix} \hat{\psi}_1(x) \\ \hat{\psi}_2(x) \\ \hat{\psi}_3(x) \end{bmatrix}. \tag{31}$$

4.2. Element formulation

By using the shape-functions defined by Eqs. (30) and (31) the approximations,

$$\int \nabla\delta\psi^*\nabla\psi \,\mathrm{d}V = \iint \delta\hat{\boldsymbol{\psi}}^H \frac{\partial \mathbf{N}_f}{\partial y}\frac{\partial \mathbf{N}_f^{\mathrm{T}}}{\partial y}\hat{\boldsymbol{\psi}} + \delta\hat{\boldsymbol{\psi}}^H \frac{\partial \mathbf{N}_f}{\partial z}\frac{\partial \mathbf{N}_f^{\mathrm{T}}}{\partial z}\hat{\boldsymbol{\psi}} \,\mathrm{d}A\,\mathrm{d}x + \iint \frac{\partial\delta\hat{\boldsymbol{\psi}}^H}{\partial x}\mathbf{N}_f\mathbf{N}_f^{\mathrm{T}}\frac{\partial\hat{\boldsymbol{\psi}}}{\partial x}\,\mathrm{d}A\,\mathrm{d}x \tag{32}$$

and

$$\int \delta\psi^*\psi \,\mathrm{d}V = \iint \delta\hat{\boldsymbol{\psi}}^H \mathbf{N}_f\mathbf{N}_f^{\mathrm{T}}\hat{\boldsymbol{\psi}} \,\mathrm{d}A\,\mathrm{d}x \tag{33}$$

follow. Exact expressions for differentiation and integration of polynomials in triangular coordinates are given in Ref. [25, Chapter 5]. These expressions now give,

$$\delta L_f = \rho_f \int \delta\hat{\boldsymbol{\psi}}^H \mathbf{b}_{11}\hat{\boldsymbol{\psi}} + \frac{\partial\delta\hat{\boldsymbol{\psi}}^H}{\partial x}\mathbf{b}_{00}\frac{\partial\hat{\boldsymbol{\psi}}}{\partial x} - \omega^2\delta\hat{\boldsymbol{\psi}}^H\mathbf{n}_2\hat{\boldsymbol{\psi}}\,\mathrm{d}x, \tag{34}$$

where the matrices $\mathbf{b}_{11}$, $\mathbf{b}_{00}$ and $\mathbf{n}_2$ are given by

$$\mathbf{b}_{00} = (A\mathbf{B}\mathbf{B}^{\mathrm{T}}), \tag{35}$$

$$\mathbf{b}_{11} = \int \mathbf{N}_f\mathbf{N}_f^{\mathrm{T}}\,\mathrm{d}A \tag{36}$$

and

$$\mathbf{n}_2 = \frac{1}{c_f^2}\mathbf{b}_{11}. \tag{37}$$

The matrix $\mathbf{B}$ is evaluated as,

$$\mathbf{B} = \begin{bmatrix} \frac{\partial \mathbf{N}_f}{\partial z} & \frac{\partial \mathbf{N}_f}{\partial y} \end{bmatrix} = \frac{1}{2A} \begin{bmatrix} (y_2 - y_3) & (z_3 - z_2) \\ (y_3 - y_1) & (z_1 - z_3) \\ (y_1 - y_2) & (z_2 - z_1) \end{bmatrix}, \tag{38}$$

where z_i and y_i, $i = 1, 2, 3$, are the coordinates of node i and A is the total area of the triangular cross-section.

5. Coupling element

5.1. Shape functions for plate strip

The shape functions for the plate strip is given in Section 3.3. The only displacement that couples to the fluid is the out of plane motion w given by Eq. (20).

5.2. Shape functions for fluid

Let the surface between node-line 1 and node-line 2 of a fluid element wet a shell element. The triangular coordinates ξ_1 and ξ_2 vary linearly over this surface. Hence, the fluid velocity potential is also interpolated by the shape functions,

$$\psi = [\tfrac{1}{2}(1 - \vartheta) \ \tfrac{1}{2}(1 + \vartheta)] \begin{bmatrix} \hat{\psi}_1(z) \\ \hat{\psi}_2(z) \end{bmatrix} = \mathbf{N}_p^{\mathrm{T}}(\vartheta)\hat{\boldsymbol{\psi}}. \tag{39}$$

Hence, the shape functions for $\hat{\psi}$ along the wetted surface may be written with the same coordinate, ϑ, as the out of plane displacement. The integration required from Eq. (11) can thus easily be made.

5.3. Coupling element formulation

With the interpolations for ψ and w described in the previous sections, the sought coupling element is given by

$$\delta B_{fc} = \mathrm{i}\omega \int [\delta\hat{\boldsymbol{\psi}}^H \ \ \delta\hat{\mathbf{w}}^H]\mathbf{m}_1 \begin{bmatrix} \hat{\boldsymbol{\psi}} \\ \hat{\mathbf{w}} \end{bmatrix} \mathrm{d}x, \tag{40}$$

where

$$\mathbf{m}_1 = \rho_f \begin{bmatrix} \mathbf{0} & \mathbf{I}_3 \\ -\mathbf{I}_3^{\mathrm{T}} & \mathbf{0} \end{bmatrix}, \tag{41}$$

where $\mathbf{0}$ is a zero matrix and the integral,

$$\mathbf{I}_3 = a \int_{-1}^{+1} \mathbf{N}_p(\vartheta)\mathbf{N}_b^{\mathrm{T}}(\vartheta)\,\mathrm{d}\vartheta, \tag{42}$$

where a is half the width of the elements of the wetted surface.

6. Equation for wave solutions

Straight but otherwise arbitrary shaped waveguides are modelled by assembling several waveguide finite elements. The assembling procedure sets degrees of freedom of shared node-lines of adjacent elements equal, and is treated in text-books on finite elements.

The assembling here is made for the plate model such that element matrices $\mathbf{a}_{00}$ are assembled into a matrix $\mathbf{A}_{00}$, likewise the fluid element matrices $\mathbf{b}_{00}$ form a matrix $\mathbf{B}_{00}$. These two matrices are then used as diagonal

blocks in the matrix

$$\mathbf{C}_{00} = \begin{bmatrix} \mathbf{B}_{00} & \mathbf{0} \\ \mathbf{0} & \mathbf{A}_{00} \end{bmatrix}. \tag{43}$$

In the same manner, other matrices $\mathbf{C}_{kl}$ for k and $l = 0, 1, 2$ and the matrix $\mathbf{M}_2$ can be formed. If there are no corresponding element matrices the blocks will be zero. Finally, the coupling element matrices $\mathbf{m}_1$ forms the antisymmetric coupling matrix $\mathbf{M}_1$.

After assembling waveguide finite elements for the fluid, the shell and the fluid–shell coupling, an approximation of Eq. (3) for a shell structure with contained fluid is given by

$$\int \sum_{k=0}^{2} \sum_{l=0}^{2} \frac{\partial^k \delta \hat{\mathbf{U}}^H}{\partial x^k} \mathbf{C}_{kl} \frac{\partial^l \hat{\mathbf{U}}}{\partial x^l} + \mathrm{i}\omega \delta \hat{\mathbf{U}}^H \mathbf{M}_1 \hat{\mathbf{U}} - \omega^2 \delta \hat{\mathbf{U}}^H \mathbf{M}_2 \hat{\mathbf{U}} \, \mathrm{d}x = \mathbf{0}. \tag{44}$$

where the vector $\hat{\mathbf{U}}(x)$ contains the degrees of freedom in the assembled fluid–shell system. Here, Eq. (44) is termed the '*weak form*' of the system equation.

Thus, by setting $\mathbf{M}_1 = 0$, two separate models emerge, for the fluid and shell systems, respectively. Rigid boundary conditions are then fulfilled for the fluid system. Also there is no distributed pressure acting on the shell system when $\mathbf{M}_1 = 0$.

By repeated integration by parts of Eq. (44), while neglecting the natural boundary terms, and subsequent usage of the calculus of variations, the weak form is transformed into, what may be referred to as, the '*strong form*' of the system equation,

$$\left[\sum_{j=0}^{4} \mathbf{K}_j \frac{\partial^j}{\partial x^j} + \mathrm{i}\omega \mathbf{M}_1 - \omega^2 \mathbf{M}_2 \right] \hat{\mathbf{U}} = \mathbf{0}, \tag{45}$$

where

$$\mathbf{K}_j = \sum_{k=0}^{2} ((-1)^{j-k} \mathbf{C}_{(j-k)k}), \quad k \leqslant j \leqslant 4. \tag{46}$$

For the straight elements utilized here Eq. (46) gives,

$$\mathbf{K}_0 = \mathbf{C}_{00}, \tag{47}$$

$$\mathbf{K}_1 = \mathbf{C}_{01} - \mathbf{C}_{10}, \tag{48}$$

$$\mathbf{K}_2 = \mathbf{C}_{02} + \mathbf{C}_{20} - \mathbf{C}_{11}, \tag{49}$$

$$\mathbf{K}_3 = \mathbf{0} \tag{50}$$

and

$$\mathbf{K}_4 = \mathbf{C}_{22}. \tag{51}$$

It may be noted that in contrast to previous work by Astley et al. [10,11], the matrix $\mathbf{K}_1 \neq \mathbf{0}$, since in-plane motion in the shell is included here.

In the absence of damping and external forces, propagating wave solutions are given as

$$\hat{\mathbf{U}} = \tilde{\mathbf{U}} \mathrm{e}^{-\mathrm{i}\kappa x}, \tag{52}$$

Inserting this into Eq. (45) gives the eigenvalue problem,

$$[\mathbf{K}(\kappa) + \mathrm{i}\omega \mathbf{M}_1 - \omega^2 \mathbf{M}_2] \hat{\mathbf{U}} = \mathbf{0}, \tag{53}$$

where

$$\mathbf{K}(\kappa) = \sum_{j=0}^{4} \mathbf{K}_j (-\mathrm{i}\kappa)^j. \tag{54}$$

Eq. (53) is a 'twin valued' eigenproblem with solutions either for a known frequency, ω, or for a known wavenumber, κ. For either problem, Eq. (53) is expanded to a larger system before the eigenproblem is solved, see e.g. Ref. [26]. For a system with N degrees of freedom the known-frequency problem yields up to $4N$ solutions, whereas the known-wavenumber problem yields $2N$ solutions. If no coupling is included, $\mathbf{M}_1 = 0$, and ω can be solved from an ordinary generalized eigenproblem.

Propagating waves are often of larger importance than decaying waves. If only propagating waves are sought, the formulation given by Eq. (53) is in a convenient form in that $\mathbf{K}(\kappa)$ is Hermitian and positive definite (except from possible rigid body motions for $\kappa = 0$). Furthermore $i\omega\mathbf{M}_1$ is Hermitian and $\mathbf{M}_2$ is real symmetric and positive definite. A system with these characteristics may be denoted as 'gyroscopic' and the system may be linearized into an Hermitian system, which also has the advantage of having orthogonal eigenvectors, see Ref. [14, Chapter 1].

In the following, dispersion curves are given for a water-filled steel pipe and for a water-filled steel duct.

7. Examples

7.1. Fluid-filled steel pipe

Equations for fluid-filled pipes with full coupling between the fluid and the shell are found in several references, e.g. Refs. [1,3]. Here the method derived by Finnveden [2] are used to validate the presented method. Finnveden uses trigonometric functions with respect to the circumference, for a circular pipe these represents an exact modal decomposition. For the radial dependence high-order polynomials are used by Finnveden. This gives a high accuracy and results from the method described in Ref. [2] with a 6th order polynomial for the radial dependence is used as reference in the following.

The material parameters are given in Table 1. These values are chosen such that the fluid shell coupling significantly affects both the predominantly fluid waves as well as the predominantly structural waves.

Two different meshes are used for waveguide FE models. These are seen in Fig. 4. The coarser mesh has 16 plate-strip elements and 32 fluid elements. The finer mesh has 32 plate-strip elements and 256 fluid elements. This corresponds to a total of 121 and 337 degrees of freedom, respectively. Note that these, automatically generated, meshes are not entirely symmetric with respect to the y and z-axes. As a result, for some of the

Table 1
Parameters used for fluid-filled pipe model

Young's modulus	E	210 GPa
Poisson's ratio	ν	0.3
Shell density	ρ	7800 kg/m^3
Shell thickness	h	5 mm
Pipe radius	r	0.1 m
Fluid sound speed	c_f	1500 m/s
Fluid density	ρ_f	1000 kg/m^3

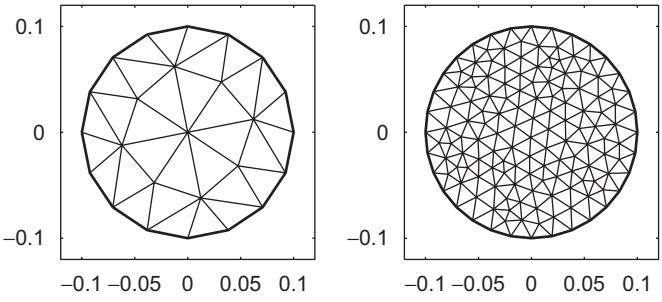

Fig. 4. Meshes for fluid-filled pipe.

dispersion relations, the waveguide FE models yield two slightly separated wavenumbers for each wavenumber found in a perfectly symmetric pipe. Here these differences are at most 0.2% and the frequencies tabulated in Table 2, relate to the average of each frequency pair. Frequencies in italics correspond to predominantly fluid waves. The dispersion curves are also plotted in Fig. 5.

The frequencies written in italics in Table 2, correspond to predominantly plane fluid cross-sectional waves. If no coupling was present, these waves would be completely plane. The wave shape in the fluid for the wave at $\kappa = 1\,\mathrm{m}^{-1}$ at approximately 200 Hz (from the coarse mesh model) is seen in Fig. 6. This wave shape shows an approximately half-sine shape over the diameter. For the coarse mesh this half-wavelength is approximated with 6 elements only. Simultaneously, the shell undergoes a simple breathing motion, approximated by 16 plate-strip elements. Since more fluid elements means more shell elements, this observation indicates that very large systems may be needed for resolving the velocity potential in the fluid. Higher order polynomials for the shape-functions of the fluid elements are likely to improve the convergence and hence the computational efficiency, in such cases. This is, however, not within the scope of this paper.

7.2. Fluid-filled steel duct

As a further example of the use of the presented method, dispersion curves for a water filled steel duct are presented. The dimensions of the duct are chosen according to the European EN 10219, standard for hollow steel profiles. The mesh used for the model is seen in Fig. 7 and the duct parameters used are given in Table 4.

Table 2
Frequencies in Hz for different wavenumbers in m^{-1}

κ	Finnveden	Coarse mesh	Fine mesh
0	235.00	243.74	237.56
0	712.00	749.72	721.62
1	38.24	37.96	38.17
1	*199.55*	*200.12*	*199.70*
1	236.53	244.68	238.51
1	512.36	509.02	511.54
2	148.20	147.16	147.94
2	243.37	251.49	245.41
2	*398.91*	*400.08*	*399.21*
2	715.98	753.54	725.39

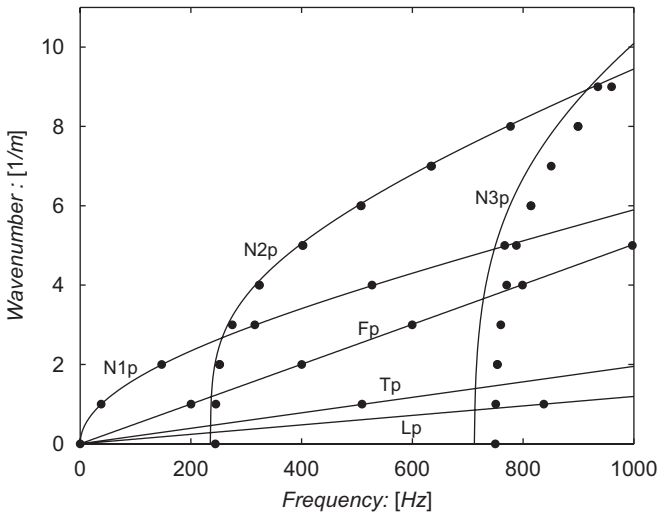

Fig. 5. Dispersion relation for fluid-filled pipe; (–) Ref. [2]; (•) Waveguide–FE coarse mesh.

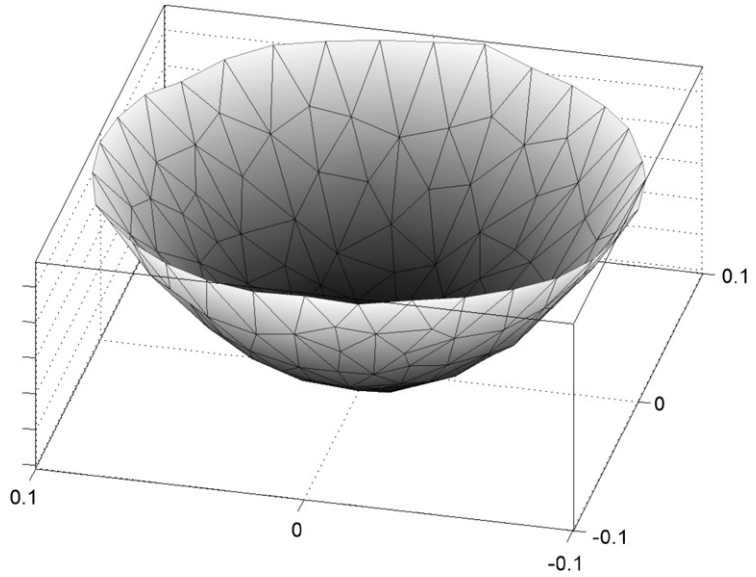

Fig. 6. Mode in fluid (velocity potential) for wave at $\kappa = 1\,\mathrm{m}^{-1}$ and frequency $f \approx 200\,\mathrm{Hz}$.

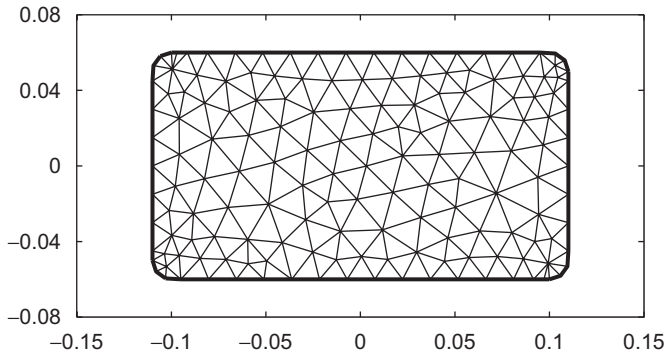

Fig. 7. Mesh of duct.

Table 3
Tabulated frequencies of lowest order wave in duct

Wavenumber $\kappa\,(\mathrm{m}^{-1})$	Frequency f (Hz)
0	0.00
1	29.90
2	111.08
3	205.61
4	267.68
5	299.40

The dispersion curves up to a wavenumber $5.5\,\mathrm{m}^{-1}$ and frequency up to 760 Hz are seen in Fig. 8. Waves propagating from zero frequency are; the 'plane' fluid wave, indicated with an 'F' in Fig. 8; the vertical and lateral 'bending' waves, indicated with 'B1' and 'B2', a torsional wave 'T', and the longitudinal wave 'L' in the shell. For reference, some values of the dispersion curve of the first bending wave, 'B1' are listed in Table 3.

Table 4
Parameters used for fluid-filled duct model

Young's modulus	E	210 GPa
Poisson's ratio	v	0.3
Shell density	ρ	7800 kg/m^3
Shell thickness	h	5 mm
Width	w	0.22 m
Height	h	0.12 m
Corner radius	r_c	0.01 m
Fluid sound speed	c_f	1500 m/s
Fluid density	ρ_f	1000 kg/m^3

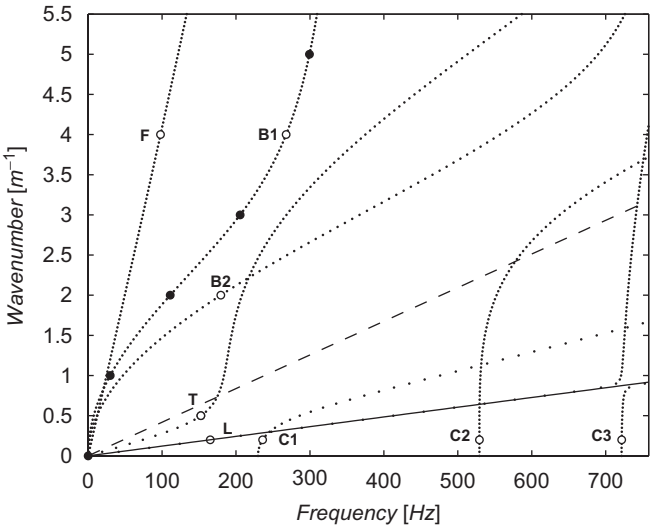

Fig. 8. Dispersion curves for fluid-filled duct; large black dots indicates tabulated values; letters indicates cross-sectional mode-shapes shown in other figures at positions given by white circles; the thin dotted line indicate plane fluid waves in water and the thin solid line indicate quasi-longitudinal waves in steel.

At higher frequencies several more waves cut-on. The first three of these waves, indicated with 'C1', 'C2' and 'C3' in Fig. 8, cuts-on at about 230, 529 and 721 Hz.

Mode-shapes, as given for the indicated points in Fig. 8, are seen in Figs. 9–17. Since there are no higher order predominantly fluid waves in the considered frequency range, the fluid velocity potential follows the displacement of the shell much according to Eq. (9). The velocity potential is thus plotted once only (in Fig. 11).

A comparison between the dispersion curves for the duct and those for the pipe shows several similarities. Predominantly longitudinal, torsional and bending waves are found in both Figs. 8 and 5.

The straight line, 'Lp', with the lowest incline in Fig. 5 corresponds to a predominantly longitudinal structural wave in the pipe, much like the 'L' wave in the duct. The straight line, 'Tp', corresponds to the torsional wave in the pipe. The dispersion curve for the predominantly fluid wave is seen as the third straight line, 'Fp', from the bottom in Fig. 5. The dispersion curve for the predominantly 'Euler-beam' flexural waves, 'N1p', are seen as the first curved line in Fig. 5, whereas higher order, predominantly structural, waves ,'N2' and 'N3', are 'cut-on' at 235 and 712 Hz. If φ is an angular coordinate around the pipe, then the 'N1', 'N2' and 'N3' waves have a circumferential dependence, $\propto \cos(n\varphi)$ for $n = 1$, 2 and 3.

One difference is that, seemingly, a pipe has only four dispersion curves starting from the origin, whereas the duct has five. This is due to the symmetry of a pipe cross-section which means that the two 'Euler-beam' flexural waves with displacements in the y- and z-directions cannot be separated. The same is true for the 'N2p' and 'N3p' waves. Hence there are actually two dots in Fig. 5 for each wavenumber for these waves.

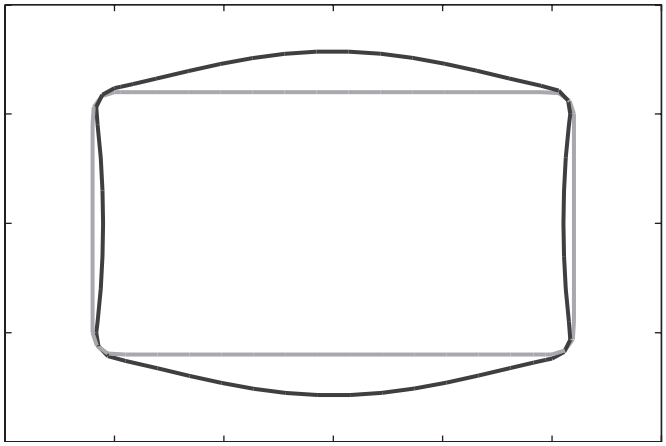

Fig. 9. Mode-shape of shell displacement at $\kappa = 4.0\,\mathrm{m}^{-1}$, $f = 97.95\,\mathrm{Hz}$, indicated with 'F' in Fig. 8.

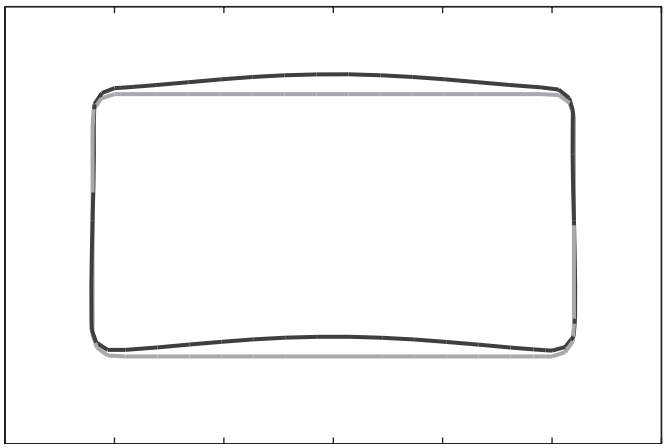

Fig. 10. Mode-shape of shell displacement at $\kappa = 4.0\,\mathrm{m}^{-1}$, $f = 267.68\,\mathrm{Hz}$, indicated with 'B1' in Fig. 8.

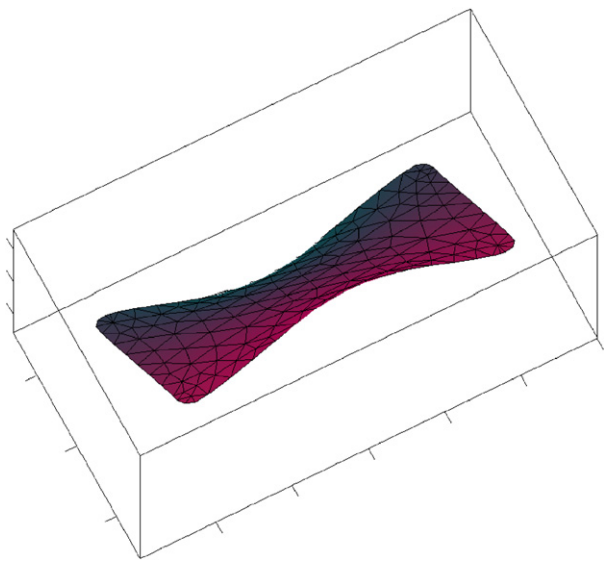

Fig. 11. Mode-shape of fluid velocity potential at $\kappa = 4.0\,\mathrm{m}^{-1}$, $f = 267.68\,\mathrm{Hz}$, indicated with 'B1' in Fig. 8.

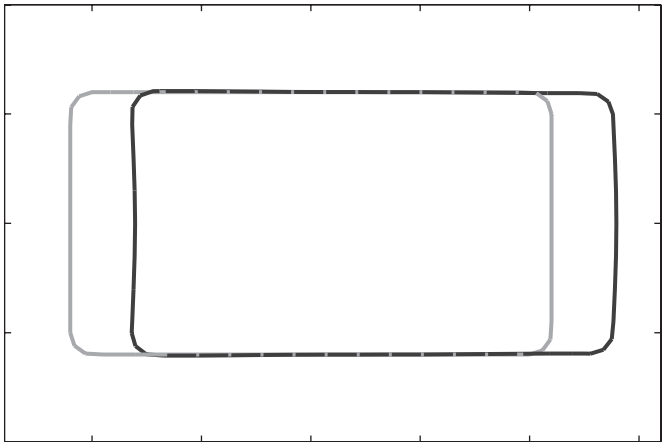

Fig. 12. Mode-shape of shell displacement at $\kappa = 2\,\mathrm{m}^{-1}$, $f = 179.42\,\mathrm{Hz}$, indicated with 'B2' in Fig. 8.

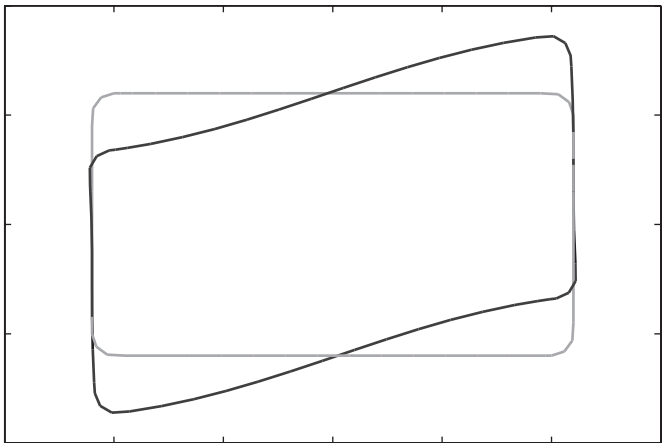

Fig. 13. Mode-shape of shell displacement at $\kappa = 0.5\,\mathrm{m}^{-1}$, $f = 152.46\,\mathrm{Hz}$, indicated with 'T' in Fig. 8.

A second difference is to be found when considering the speed of the predominantly fluid wave in the two cases, i.e. the slope of the straight lines indicating the predominantly 'plane' fluid waves.

In Fig. 8, two lines indicating the 'quasi-longitudinal' wave in steel (solid) and plane fluid wave in water (dashed) are shown together with the dispersion curves. It can be seen that the fluid coupling on the longitudinal wave would be negligible for most practical applications whereas the coupling's effect on the fluid wave reduces the sound speed to about a tenth compared to the sound speed for a case with rigid walls. This can be explained with a high flexibility of the duct walls when subjected to an internal pressure. In contrast, for a perfect circular pipe, the displacement due to an increased pressure is resisted with the in-plane stiffness of the shell and the walls then present a nearly rigid boundary for the fluid.

A third difference is that, for the pipe, as may be noticed from Fig. 5, the different dispersion curves always cross each other. These crossings are related to orthogonal modes and are less often found in more general waveguides. For a pipe, due to the axi-symmetry, the wave-shapes may be described with trigonometric dependence about the circumference, and as a consequence, all the wave-shapes are clearly orthogonal.

For the duct case, the dispersion curves cross each other at the intersections (F,B2), (F,B1), (T,B2) , (L,C1) and (L,C2). These crossings can also be explained by orthogonal wave shapes. This in turn is due to the fact that the cross-section of the duct is symmetric both with respect to the y-axis and with respect to the z-axis. Hence all waves are either symmetric or anti-symmetric with respect to these axes, very much like ordinary modes. An anti-symmetric wave shape is clearly orthogonal to a symmetric wave shape. The symmetry and

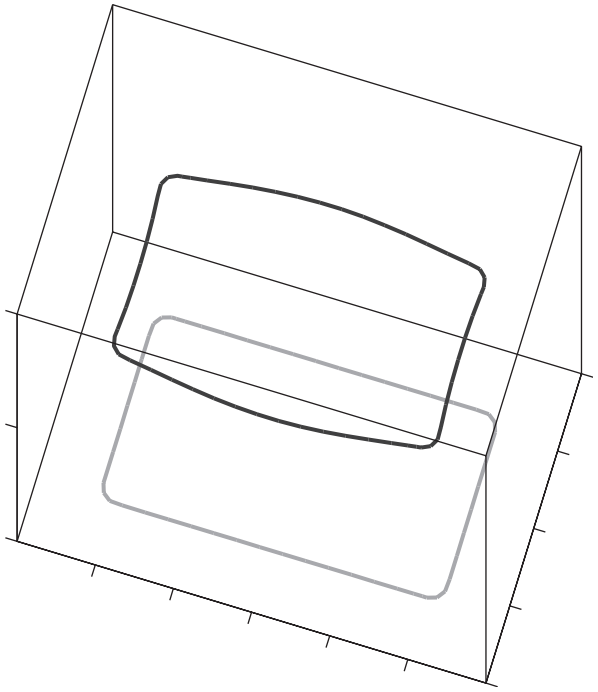

Fig. 14. Mode-shape of shell at $\kappa = 0.2\,\mathrm{m}^{-1}$, $f = 165.18\,\mathrm{Hz}$, indicated with 'L' in Fig. 8.

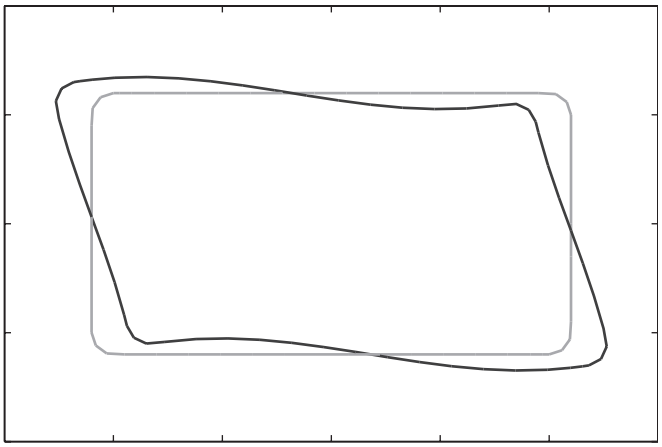

Fig. 15. Mode-shape of shell at $\kappa = 0.2\,\mathrm{m}^{-1}$, $f = 236.01\,\mathrm{Hz}$, indicated with 'C1' in Fig. 8.

anti-symmetry of the waves are clearly seen in Figs. 9–15. However, when two waves have the same type of symmetry or anti-symmetry, as is the case for the 'T' wave and the 'C1' wave pair and for the 'L' and 'C3' wave pair, the two dispersion curves 'repel' each other. This phenomena, often referred to as curve veering, is reported in several papers e.g. Refs. [27,28].

The 'L' and 'C3' veering is further investigated in Figs. 18 and 19. It is noted that the modeshape of the 'L' wave at position 'A' (before the veering) is slightly different from that shown previously in Fig. 14. This difference has however been found to be a gradual change rather than a phenomenon associated with the curve crossing of 'L' with the dispersion curves 'C1' and 'C2'. In contrast, the veering to the 'C3' curve introduces a rapid change in the modeshape of the 'L' wave. In a frequency range close to the veering the 'L' and 'C3' waves have similar modeshapes, the only noticeably difference is that the 'L' wave have a significant

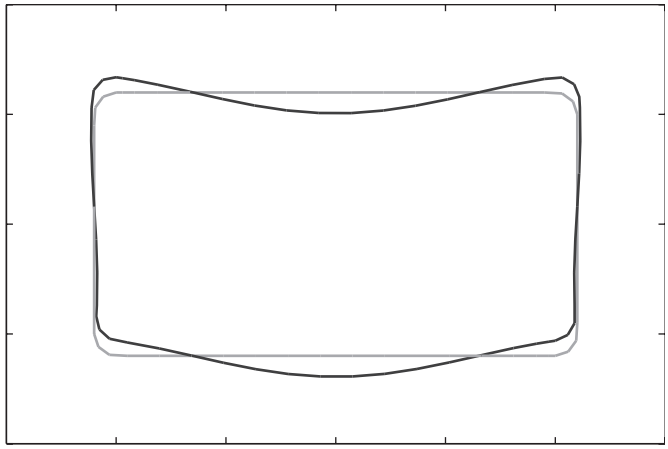

Fig. 16. Mode-shape of shell at $\kappa = 0.2\,\mathrm{m}^{-1}$, $f = 529.16\,\mathrm{Hz}$, indicated with 'C2' in Fig. 8.

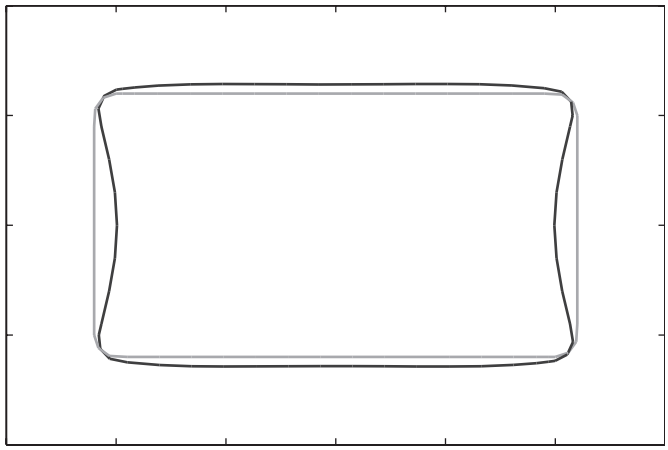

Fig. 17. Mode-shape of shell at $\kappa = 0.2\,\mathrm{m}^{-1}$, $f = 721.67\,\mathrm{Hz}$, indicated with 'C3' in Fig. 8.

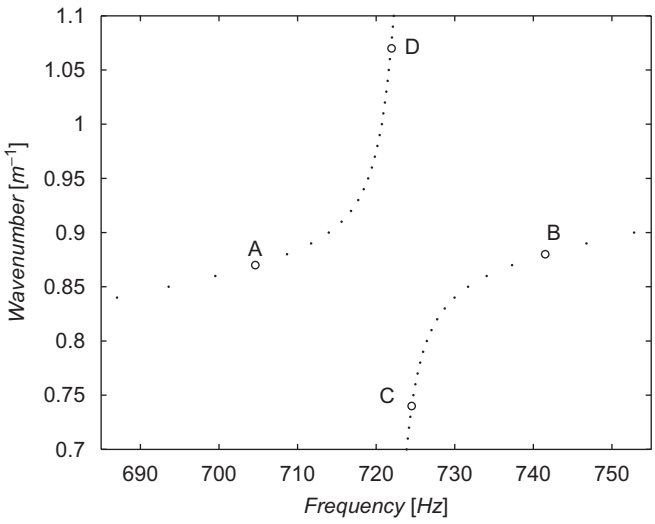

Fig. 18. Dispersion relation at curve veering.

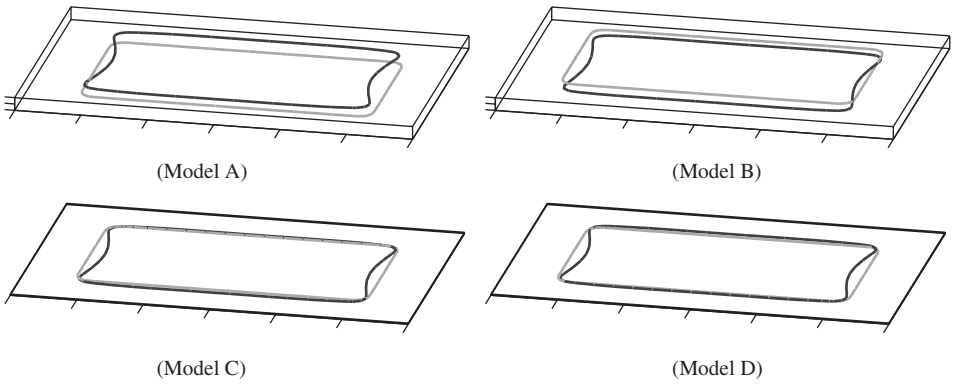

Fig. 19. Waves at the curve veering about 720 Hz. Notations corresponding to Fig. 18; Mode 'A' at $\kappa = 0.87\,\mathrm{m}^{-1}$, $f = 704.61$ Hz; Mode 'B' at $\kappa = 0.88\,\mathrm{m}^{-1}$, $f = 741.52$ Hz; Mode 'C' at $\kappa = 0.74\,\mathrm{m}^{-1}$, $f = 724.53$ Hz; Mode 'D' at $\kappa = 1.07\,\mathrm{m}^{-1}$, $f = 721.89$ Hz.

longitudinal displacement. At the veering this longitudinal displacement is transferred from the to 'AC' curve to the 'BD' curve. The relative phase between the displacement within the cross-section and the longitudinal displacement has also changed. It has been found that at position 'A' the x-displacements are almost in phase with the sidewalls contraction, whereas at position 'B' they are in phase with the sidewalls expansion.

8. Conclusions

Waveguide finite elements for fluid and fluid–shell coupling are presented. Together with previously derived plate-strip elements, which here have the in-plane motion enriched, equations for fully coupled fluid-filled ducts and pipes can be found. Two examples, one for a pipe and one for a duct with close to rectangular cross-section are presented. Dispersion curves and some wave-shapes for these examples are shown.

Comparing the dispersion curves for the pipe with those obtained from a previously presented method for fluid-filled pipes, [2], it is found that the results agree well although the waveguide-FE approach has a slower rate of convergence, which is explained by the linear approximating space used for the fluid elements. The dispersion curves for the near rectangular water-filled duct provides a novel example of a result that would be difficult to calculate with analytical methods. The same branches as for the circular pipe are recognized, though, of course, the dispersion curves and the mode shapes are largely different. In particular, the almost plane, predominantly fluid mode has a much lower speed of propagation because of the higher flexibility of the almost flat shell wall.

The waveguide finite element method is a very useful tool for analysis of Vibro-acoustic motion and the presented elements largely increase the class of structure for which it can be used. As an example, using the elements presented here, and slightly modified versions of these, the authors are currently analysing the response of car tyres, double walls, embedded rails, railway car structures and a loudspeaker.

References

[1] C.R. Fuller, F.J. Fahy, Characteristics of wave propagation in cylindrical elastic shells filled with fluid, *Journal of Sound and Vibration* 81 (1) (1982) 501–518.
[2] S. Finnveden, Spectral finite element analysis of the vibration of straight fluid-filled pipes with flanges, *Journal of Sound and Vibration* 199 (1) (1996) 125–154.
[3] G. Pavič, Vibroacoustical energy flow through straight pipes, *Journal of Sound and Vibration* 54 (1992) 411–429.
[4] N. Wagner, M. Maess, L. Gaul, Dispersion curves of fluid filled elastic pipes by standard fe models and eigenpath analysis, *Journal of Sound and Vibration* 296 (2006) 264–276.
[5] S. Finnveden, Evaluation of modal density and group velocity by a finite element method, *Journal of Sound and Vibration* 273 (2004) 51–75.
[6] C.M. Nilsson, S. Finnveden, *Journal of Sound and Vibration* 305 (4) (2007) 641–658.
[7] F. Birgersson, S. Finnveden, C.M. Nilsson, *Journal of Sound and Vibration* 287 (1) (2005) 297–314.

[8] B. Alaami, Waves in prismatic guides of arbitrary cross section, *Journal of Applied Mechanics* 40 (1973) 1067–1071.
[9] V.V. Volovoi, D.H. Hodges, V.L. Berdichevski, V.G. Sutyrin, Dynamic dispersion curves for non-homogeneous, anisotropic beams with cross sections of arbitrary geometry, *Journal of Sound and Vibration* 215 (5) (1998) 1101–1120.
[10] R.J. Astley, A. Cummings, N. Sormaz, A finite element scheme for acoustic propagation in flexible-walled ducts with bulk-reacting liners, and comparison with experiment, *Journal of Sound and Vibration* 150 (1) (1991) 119–138.
[11] R.J. Astley, A. Cummings, A finite element scheme for acoustic transmission through the walls of rectangular ducts: comparison with experiment, *Journal of Sound and Vibration* 92 (1984) 387–409.
[12] R. Kirby, Transmission loss predictions for dissipative silencers of arbitrary cross section in the presence of mean flow, *Journal of the Acoustical Society of America* 112 (1) (2003) 200–209.
[13] L. Gavric, Finite-element computation of dispersion properties of thin-walled waveguides, *Journal of Sound and Vibration* 173 (1) (1994) 113–124.
[14] C.-M. Nilsson, Waveguide Finite Elements Applied on a Car Tyre, PhD Thesis, Royal Institute of Technology, Aeronautical and Vehicle Engineering/MWL, 2004. TRITA-AVE 2004:21, ISBN 91-7283-798-5, http://media.lib.kth.se/dissengrefhit. asp?dissnr = 3812i.
[15] A. Cummings, Sound transmission through duct walls, *Journal of Sound and Vibration* 4 (2001) 731–765.
[16] L. Houillon, M.N. Ichchou, L. Jezequel, Wavemotion in thin-walled structures, *Journal of Sound and Vibration* 281 (2005) 483–507.
[17] B.R. Mace, D. Duhamel, M.J. Brennan, L. Hinke, Finite element prediction of wave motion in structural waveguides, *Journal of the Acoustical Society America* 117 (5) (2005) 2835–2843.
[18] Y. Waki, B.R. Mace, M.J. Brennan, Waveguide finite element modelling; numerical issues and application to simple waveguides, *Proceedings of the ISMA 2006 Conference*, 2006, pp. 2435–2449.
[19] SS-EN 10219-2, cold formed structural hollow sections of non-alloy and fine grain steels—part 2: tolerances, dimensions and sectional properties, Swedish Standards Institute, 1998.
[20] L.G. Olson, K.-J. Bathe, Analysis of fluid–structure interactions, a direct symmetric coupled formulation based on the fluid velocity potential, *Computers and Structures* 21 (1/2) (1985) 21–32.
[21] G. Sandberg, P. Göransson, A symmetric finite element formulation for acoustic fluid–structure interaction analysis, *Journal of Sound and Vibration* 123 (3) (1988) 507–515.
[22] M. Petyt, *Introduction to Finite Element Vibration Analysis*, Cambridge University Press, Cambridge, 1990.
[23] S. Temkin, *Elements of Acoustics*, Wiley, New York, 1981.
[24] U. Orrenius, S. Finnveden, Calculation of wave propagation in rib-stiffened plate structures, *Journal of Sound and Vibration* 198 (2) (1996) 203–224.
[25] R.D. Cook, *Concepts and Applications of Finite Element Analysis*, second ed., Wiley, New York, 1981.
[26] F. Tisseur, K. Meerbergen, The quadratic eigenvalue problem, *SIAM Review* 43 (2) (2001) 235–286.
[27] X.L. Liu, Behavior of derivatives of eigenvalues and eigenvectors in curve veering and mode localization and their relation to close eigenvalues, *Journal of Sound and Vibration* 256 (2002) 551–564.
[28] R.A. Cairns, The role of negative energy waves in some instabilities of parallel flows, *Journal of Fluid Mechanics* 92 (1) (1979) 1–14.